Fall run 2019 – analysis report

W. Schreyer

December 12, 2019

Contents

1 Introduction

This document describes several analyses of the data taken during the 2019 run of the UCN source at TRIUMF, covering measurements of

- transmission through guide components,
- storage lifetime in the source, and
- storage lifetime in guide components.

All these experiments are performed in cycles. Each cycle contains several periods, typically starting with an irradiation period, during which the target is irradiated with protons and ultracold neutrons are produced. This can be

followed by up to 9 more periods, like storage or detection periods. For each period, up to 8 UCN components like valves or spin flippers can be to set different states. The last (11th) period covers the time until the next irradiation and cycle starts.

Cycles with different period durations and valve settings can be grouped in supercycles, which can be repeated several times. Cycles of one experiment can be spread over several Midas runs.

Two UCN detectors were used throughout the run. A Li6 detector, detecting scintillation light of UCN captured in ^{6}Li-enriched glass, and a He3 detector, detecting gas discharges due to UCN captured by ^{3}He. Experiments can use either detector alone or both at the same time.

2 Preparation of raw detector data

2.1 Trigger thresholds

The Li6 detector uses two values to determine if a detected event was actually caused by a UCN: "PSD" based on the pulse shape of the event and Q_{long}, the charge collected during a 200 ns window after the event trigger. An event is considered a UCN if

$$\text{PSD} > 0.3 \tag{1}$$

and

$$Q_{\text{long}} > 2000. \tag{2}$$

The He3 detector considers an event to be a UCN if the charge collected after the event trigger

$$Q_{\text{short}} > 300. \tag{3}$$

3 Transmission measurements

Transmission measurements are experiments with three periods per cycle. An irradiation period, t_i, where UCN are produced while the valve IV2 downstream of the He3 detector is closed. A pre-storage period t_p, where the irradiation is stopped and the source valve IV1 is closed, storing UCN between IV1 and IV2 while monitoring the rate in the He3 detector connected to this volume. And a counting period, t_c, where the UCN valve is opened and UCN transmitted through components downstream of the valve are detected in the Li6 detector.

The UCN counted in the He3 detector during the pre-storage period give a measure or how many UCN are available for transmission to the Li6 detector once IV2 opens. Hence, the ratio

$$R_p = \frac{N_c^{\text{Li6}}}{N_p^{\text{He3}}} \tag{4}$$

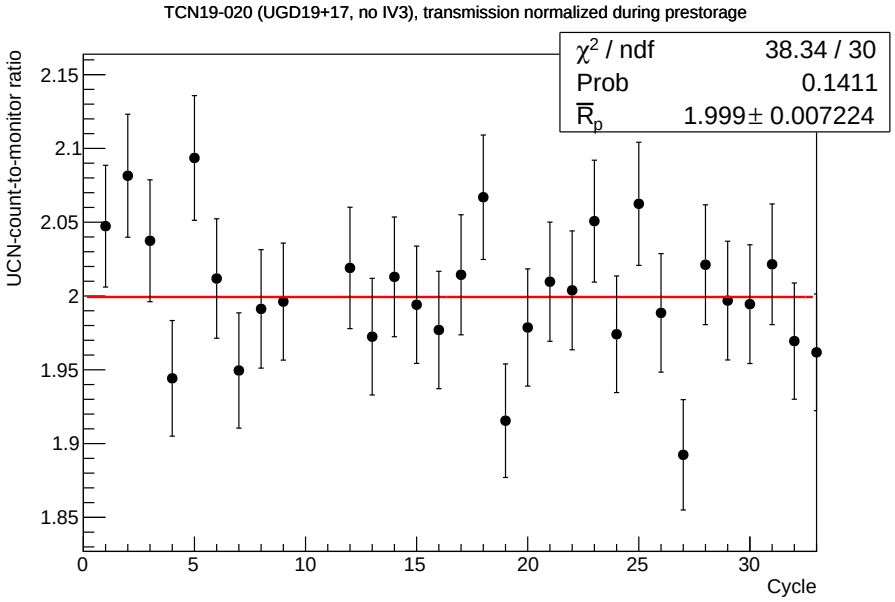

Figure 1: Ratio of Li6 counts during the counting period to He3 counts during the pre-storage period. All cycles of transmission experiment TCN19-020 are shown and fitted with a constant function. The legend shows the χ^2/ν of the fit, the average ratio $\bar{R}$, and its uncertainty.

of UCN seen in the Li6 detector N_c^{Li6} to the UCN seen in the He3 detector N_p^{He3} is a measure of how well UCN can be transmitted through the guides between the valve and the Li6 detector.

A background rate b^{Li6} estimated during the pre-storage periods is subtracted from the number of events counted in the Li6 detector during counting C_c^{Li6}:

$$N_c^{\mathrm{Li6}} = C_c^{\mathrm{Li6}} - b^{\mathrm{Li6}} \cdot t_c, \tag{5}$$

with an uncertainty

$$\Delta N_c^{\mathrm{Li6}} = \sqrt{\sqrt{C_c^{\mathrm{Li6}}}^2 + \left(\Delta b^{\mathrm{Li6}} \cdot t_c\right)^2}. \tag{6}$$

The uncertainty of the ratio R is then

$$\Delta R_c = \sqrt{\left(\frac{\Delta N_c^{\mathrm{Li6}}}{N_p^{\mathrm{He3}}}\right)^2 + \left(\sqrt{N_p^{\mathrm{He3}}}\frac{N_c^{\mathrm{Li6}}}{N_p^{\mathrm{He3}^2}}\right)^2}. \tag{7}$$

The He3 detector is assumed to be background-free.

The ratios for all cycles are plotted using ROOT. A χ^2 fit of a constant function over all cycles is used to determine the average $\bar{R}_p$ and its uncertainty

$\Delta\bar{R}_p$, see figure 1. Table 1 shows the results for all performed transmission experiments.

The relative transmission T of one experiment compared to another is

$$T_c = \frac{\bar{R}_{p1}}{\bar{R}_{p2}} \tag{8}$$

with the uncertainties for each $\bar{R}_p$ scaled by the χ^2 per degrees of freedom ν from the fit:

$$\Delta T_p = T_p \sqrt{\left(\frac{\Delta\bar{R}_{p1}\chi_1^2}{\bar{R}_{p1}\nu_1}\right)^2 + \left(\frac{\Delta\bar{R}_{p2}\chi_2^2}{\bar{R}_{p2}\nu_2}\right)^2}. \tag{9}$$

Comparisons of transmission through different guide geometries are shown in table 2.

The normalization during counting, giving ratios R_c and T_c as explained in the 2018 report, are given as comparison. The pre-storage method is considered more reliable.

3.1 Excluded cycles

Individual cycles are excluded from the analyzed pre-storage transmission data if

- no beam data was available (2 cycles);
- the beam current dropped below 0.8 µA (68 cycles);
- the beam current fluctuated by more than 0.02 µA (8 cycles);
- the last period does not contain any Li6 events, i.e. the run was aborted at some point during this cycle (71 cycles);
- IV1 never opened (5 cycles);
- the He3 detector detected no UCN during pre-storage (1 cycle);

In total, 155 out of 2166 cycles were excluded.

3.2 Systematic effect due to fluctuations in pre-storage lifetime

The transmission measurement with normalization during pre-storage is dependent on the storage lifetime in the pre-storage volume. The rate in the He3 detector, which is proportional to the number of UCN in the pre-storage volume, exponentially drops over time, see fig. 2. And the total number detected is

$$N_p^{\mathrm{He3}} = \int_0^{t_p} N_0 \exp\frac{-t}{\tau_p} dt = N_0\tau_p \left(1 - \exp\frac{-t_p}{\tau_p}\right). \tag{10}$$

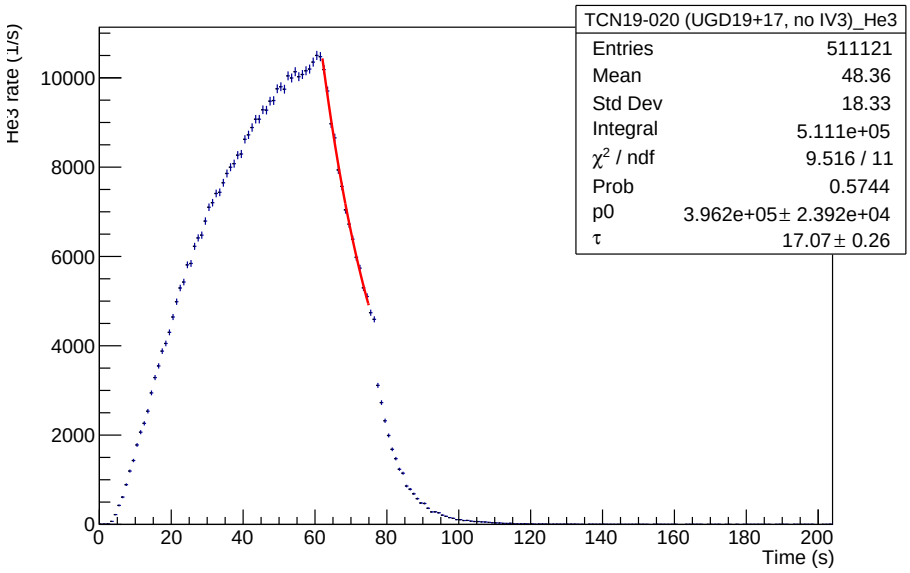

Figure 2: Rate in the He3 detector during transmission experiment TCN19-020, summed over all cycles and with an exponential fit during the pre-storage time.

The number detected in the Li6 detector is the number of UCN in the pre-storage volume at the end of the pre-storage period, multiplied with the transmission T_{corr}:

$$N_c^{\mathrm{Li6}} = T_{\mathrm{corr}} N_0 \exp \frac{-t_p}{\tau_p}. \tag{11}$$

Hence the Li6-to-He3 ratio is actually a measure of the transmission T modified with a factor dependent on τ_p:

$$\frac{N_c^{\mathrm{Li6}}}{N_p^{\mathrm{He3}}} = T_{\mathrm{corr}} \frac{\exp \frac{-t_p}{\tau_p}}{\tau_p \left(1 - \exp \frac{-t_p}{\tau_p}\right)} \tag{12}$$

This factor can be divided out by measuring the storage lifetime in the pre-storage volume by fitting an exponential decay to the falling He3 rate. However, the resulting transmission uncertainties are significantly increased.

Over time, the storage lifetime in the pre-storage volume determined this way during all standard transmission experiments with a pre-storage time of 15 s fluctuated between 16.2 s and 17.2 s, see fig. 3.

3.3 Results

Table 1 lists the results of the individual transmission experiments and table 2 compares several.

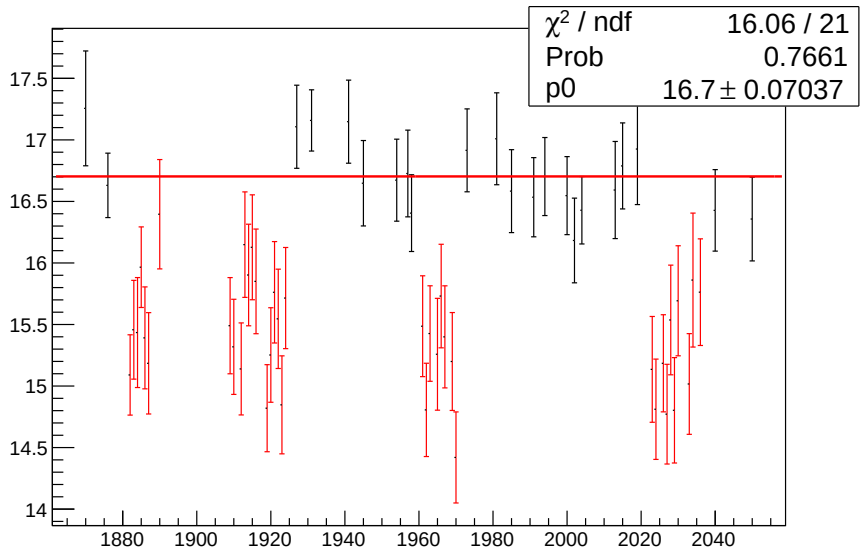

Figure 3: Storage lifetime in the pre-storage volume determined during all transmission measurements. The black data points are from measurements with a pre-storage time of 15 s, the red from DREx measurements with a pre-storage time of 10 s.

Table 1: Results of transmission experiments. If not otherwise noted, all transmission measurements were performed with the listed guides between IV2 and IV3 with their O-rings pointing towards each other and a 90° elbow downstream of IV3. The χ^2 gives an indication of how well the data fits the assumption that the ratios R stay constant over all cycles in each experiment.

Experiment	Run	$\bar{R}_p$	χ^2/ν	$\bar{R}_{\text{corr}}$	$\bar{R}_c$	χ^2/ν	Description
TCN19-020	1876	1.999 ± 0.007	1.28	48.7 ± 0.8	8.315 ± 0.030	0.61	UGD19+17, no IV3
TCN19-010	1870, 1871	1.825 ± 0.011	1.05	43.6 ± 1.2	7.571 ± 0.026	0.64	UGD19+22 (NiP)
TCN19-240	1927	1.890 ± 0.008	1.16	45.4 ± 0.9	7.792 ± 0.028	1.47	UGD02+22 (SS)
TCN19-250	1931, 1937	1.768 ± 0.006	1.01	42.4 ± 0.6	7.365 ± 0.019	1.21	UGD02+19+22 (SS+NiP)
TCN19-260	1941	1.879 ± 0.009	1.42	45.0 ± 0.9	8.045 ± 0.29	0.58	UGD22
TCN19-280v1	1945	1.848 ± 0.009	0.91	45.0 ± 1.0	7.533 ± 0.027	0.77	vent spider
TCN19-280v2	1954	1.820 ± 0.008	1.47	44.3 ± 0.9	7.719 ± 0.028	0.98	vent spider with plunger full in
TCN19-280v3	1957	1.878 ± 0.009	0.94	45.6 ± 1.0	–	–	vent spider with plunger cycled
TCN19-280v4	1958	1.835 ± 0.008	0.73	45.0 ± 0.9	–	–	vent spider with plunger full in
TCN19-010D	1973	1.810 ± 0.008	0.50	43.7 ± 0.9	7.584 ± 0.027	1.02	UGD19+22 (NiP)
TCN19-270	1981	1.408 ± 0.007	1.16	33.9 ± 0.8	4.679 ± 0.017	2.12	UGD13+14+15+22 (Cu)
TCN19-120	1985	1.804 ± 0.008	0.99	44.0 ± 0.9	7.203 ± 0.026	0.75	UGD37+22 (95mm Al-NiP)
Measurements after detector was exposed to light:							
TCN19-121	1991	1.522 ± 0.007	1.39	37.2 ± 0.8	–	–	UGD36+22 (95mm Al-NiP rough)
TCN19-123	1994	1.645 ± 0.008	0.71	40.0 ± 0.8	6.655 ± 0.026	0.94	UGD39+22 (95mm Al-NiP)
TCN19-100	2000	1.729 ± 0.008	1.99	42.2 ± 0.9	–	–	UGD31+33+22 (95mm SS-NiP)
TCN19-101	2002	1.536 ± 0.007	0.85	37.9 ± 0.8	–	–	UGD30+32+22 (95mm SS-black NiP)
TCN19-120A	2004, 2005	1.650 ± 0.007	1.35	40.4 ± 0.7	6.615 ± 0.025	1.35	UGD37+22 (95mm Al-NiP)
TCN19-102	2013	1.670 ± 0.008	0.81	40.73 ± 0.9	–	–	UGD34+35+22 (95mm Al-NiP)
TCN19-124	2015	1.680 ± 0.008	1.77	40.7 ± 0.9	–	–	UGD40+22 (95mm SS-NiP smooth)
TCN19-010E	2019	1.730 ± 0.008	1.80	41.7 ± 1.1	7.162 ± 0.027	0.58	UGD19+22 (NiP)
TCN19-120B	2040	1.631 ± 0.008	1.66	40.0 ± 0.8	–	–	UGD37+22 (95mm Al-NiP)
TCN19-010B	2050	1.683 ± 0.009	0.75	41.3 ± 0.9	–	–	UGD19+22 (NiP)

Table 2: Comparison of transmission experiments.

Experiment	Reference	T_p	T_{corr}	T_c	Description
TCN19-010	TCN19-020	0.913 ± 0.007	0.896 ± 0.029	0.911 ± 0.005	Transmission of IV3
TCN19-010	TCN19-260	0.972 ± 0.008	0.969 ± 0.034	0.941 ± 0.005	Adding UGD19
TCN19-240	TCN19-260	1.006 ± 0.007	1.007 ± 0.029	0.969 ± 0.006	Adding UGD02
TCN19-250	TCN19-260	0.941 ± 0.006	0.941 ± 0.024	0.915 ± 0.004	Adding UGD02+19
TCN19-270	TCN19-260	0.749 ± 0.006	0.752 ± 0.023	0.582 ± 0.004	Adding UGD13+14+15
TCN19-280v1	TCN19-260	0.983 ± 0.007	0.998 ± 0.029	0.936 ± 0.005	Spider compared to UGD22
TCN19-280v2	TCN19-260	0.968 ± 0.008	0.982 ± 0.028	0.960 ± 0.005	Spider compared to UGD22
TCN19-280v3	TCN19-260	0.999 ± 0.007	0.984 ± 0.029	–	Spider compared to UGD22
TCN19-280v4	TCN19-260	0.977 ± 0.007	1.012 ± 0.030	–	Spider compared to UGD22
TCN19-120	TCN19-260	0.960 ± 0.007	0.977 ± 0.028	0.895 ± 0.005	Adding UGD37
Reproducibility measurements:					
TCN19-010D	TCN19-010	0.992 ± 0.008	1.002 ± 0.034	0.998 ± 0.005	Before detector exposure
TCN19-010E	TCN19-010	0.948 ± 0.009	0.957 ± 0.037	0.946 ± 0.005	After and before exposure
TCN19-120A	TCN19-120	0.914 ± 0.006	0.919 ± 0.025	0.918 ± 0.005	After and before exposure
TCN19-010B	TCN19-010E	0.973 ± 0.008	0.991 ± 0.034	–	After and before isopure refill
TCN19-120B	TCN19-120A	0.989 ± 0.008	0.989 ± 0.027	–	After and before isopure refill
Measurements after detector was exposed to light:					
TCN19-100	TCN19-120A	1.048 ± 0.008	1.044 ± 0.028	–	SS-NiP compared to Al-NiP
TCN19-101	TCN19-120A	0.931 ± 0.006	0.938 ± 0.026	–	Black NiP compared to Al-NiP
TCN19-102	TCN19-120A	1.012 ± 0.007	1.007 ± 0.030	–	Al-NiP compared to Al-NiP
TCN19-121	TCN19-120A	0.923 ± 0.007	0.920 ± 0.025	–	Rough Al-NiP to Al-NiP
TCN19-123	TCN19-120A	0.997 ± 0.007	0.988 ± 0.026	1.006 ± 0.006	Al-NiP compared to Al-NiP
TCN19-124	TCN19-120A	1.018 ± 0.008	1.007 ± 0.028	–	Smooth SS-NiP to Al-NiP

Table 3: Roughness R_a of each guide measured with a profilometer. The definition for R_a is very sensitive to outliers, causing large variations. Struck-out outliers are excluded from the average.

Guide	Roughness (nm)								Average
UGD19	104	80	74	86	~~400~~	~~337~~	88	96	88 ± 11
UGD02	81	70	71	77	99	83			80 ± 11
UGD37	184	197	189	87	96	107			143 ± 52
UGD36	976	~~1573~~	968	850	955	926			935 ± 51
UGD39									
UGD31	64	89	82	77	116	~~492~~	94		87 ± 18
UGD33	~~608~~	130	125	~~990~~	69	63	~~633~~	~~608~~	97 ± 36
UGD30	~~970~~	198	633	1326	111	105	416		465 ± 469
UGD32	107	422	627	~~1740~~	607	140	1255	672	700 ± 598
UGD34	83	~~154~~	121	113	89	87			99 ± 17
UGD35	162	152	233	128	164	237			179 ± 45
UGD40	48	64	61	40	47	105			61 ± 23
UGD13	156	134	207	197	140	185			170 ± 31
UGD14	183	398	163	344	156	158			234 ± 108

We used a Mitutoyo SJ-210 profilometer to determine roughnesses R_a of the guides, see table 3. The transmission was clearly correlated to the roughness, see figures 4, 5—the less polished guides UGD13–15 and UGD36 showed significantly lower transmission. The guides with stainless steel substrate provided slightly lower roughnesses and potentially slightly higher transmission, but the differences become insignificant when including the pre-storage-lifetime correction.

Transmission through combinations of guides with varying total lengths paint a less clear picture. Adding the stainless-steel guide UGD02 actually seems to increase transmission, while adding the NiP-plated guide UGD19 reduces transmission by 3 %. Combining both guides doubles the loss in transmission to 6 %, see Fig. 6. Again, these effects are barely significant when including the pre-storage-lifetime correction.

4 Storage lifetime in the source

To measure the storage lifetime of UCN in the source, we performed several cycles with three periods each. During the first period, the target is irradiated to accumulate UCN in the source with IV1 closed. During the second period, the beam is turned off and the UCN are stored with IV1 closed. In the third period, the valve is opened and the UCN stored in the source are emptied into the detector(s). This cycle is repeated several times with varying duration of the storage period. This measurement was repeated regularly to determine the change of storage lifetime over time.

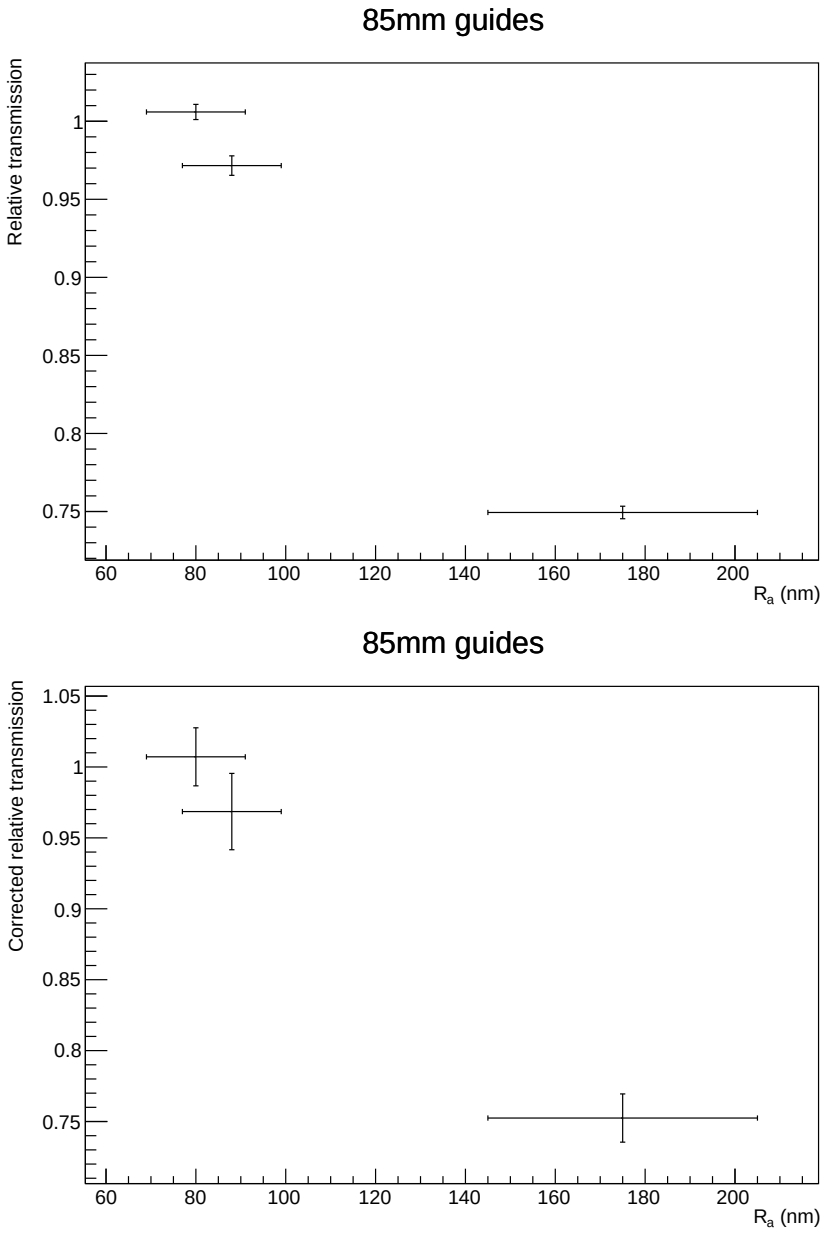

Figure 4: Transmission T_p (top) and corrected transmission T_{corr} (bottom) through 85 mm-diameter guides with different roughnesses.

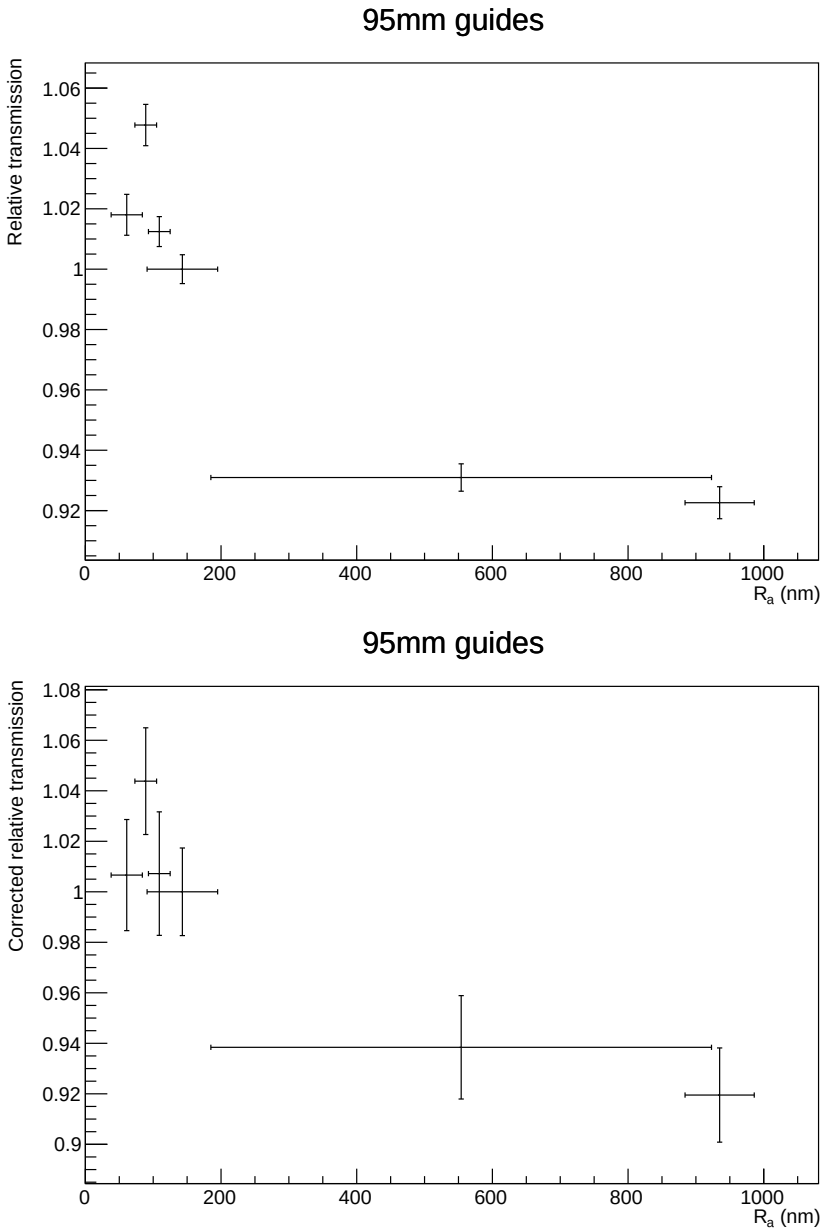

Figure 5: Transmission T_p (top) and corrected transmission T_{corr} (bottom) through 95 mm-diameter guides with different roughnesses.

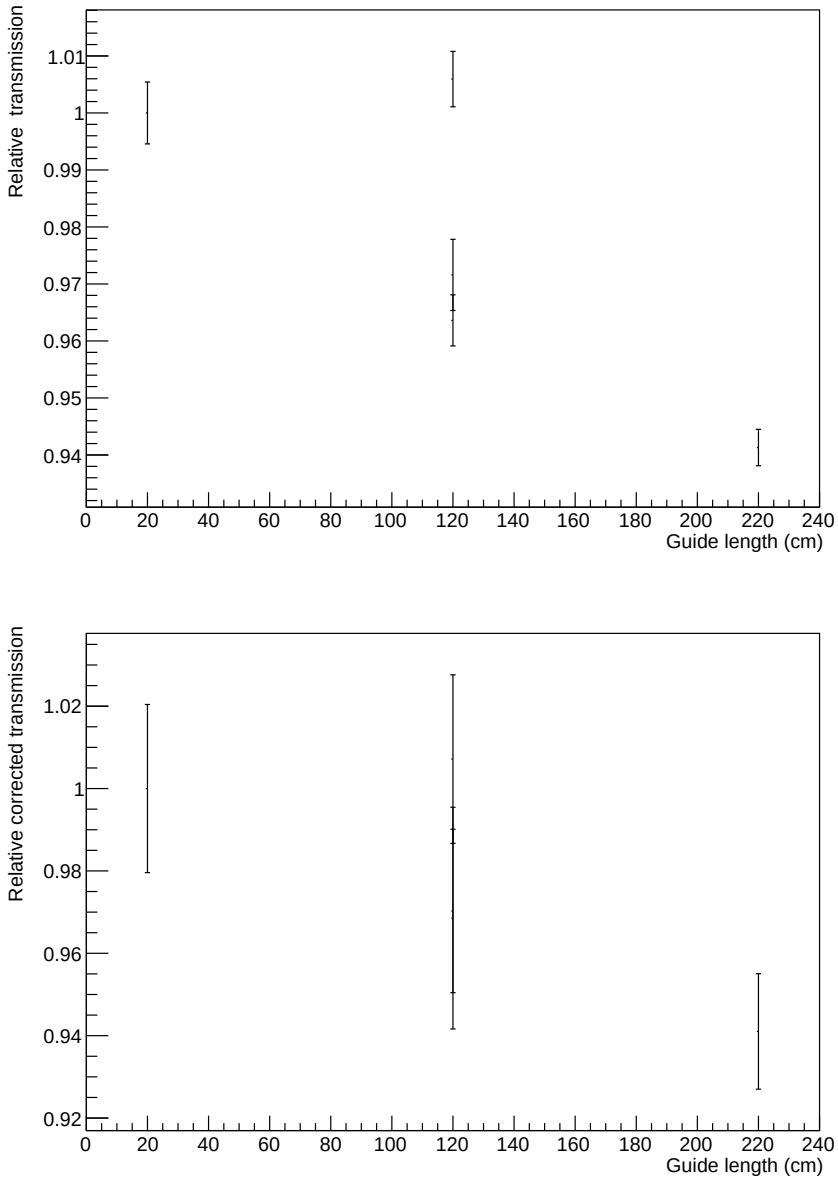

Figure 6: Transmission T_p (top) and corrected transmission $T_{\rm corr}$ (bottom) through combinations of 85 mm-diameter guides with different total lengths.

To determine the storage lifetime, we subtracted the average background rates determined during the storage period, see equation 5, from the events in the respective detector, and divided it by the average beam current $\bar{I}$ during irradiation:

$$n_c = \frac{N_c}{\bar{I}}. \tag{13}$$

To take into account fluctuations of the beam current, its standard deviation during irradiation ΔI is included in the uncertainty

$$\Delta n_c = n_c \sqrt{\left(\frac{\Delta N_c}{N_c}\right)^2 + \left(\frac{\Delta I}{\bar{I}}\right)^2}. \tag{14}$$

Ideally, the number of detected UCN should drop exponentially with increasing storage time and the exponential time constant is the storage lifetime, see fig. 7. Compared to 2018, however, the source seemed to operate more stably with smaller changes of liquid-helium temperatures and smaller fluctuations of the UCN yield.

4.1 Excluded cycles

Individual cycles are excluded from the analyzed storage-lifetime data if

- no beam data was available (2 cycles);
- the beam current dropped below 0.1 µA (7 cycles);
- the beam current fluctuated by more than 0.02 µA (1 cycle);
- the last period does not contain any Li6 events, i.e. the run was aborted at some point during this cycle (11 cycles);
- IV1 never opened (6 cycles); or
- no events were detected during the irradiation period (1 cycle).

In total, 28 out of 351 cycles had to be excluded.

4.2 Change of storage lifetime over time

The storage lifetime in the source seemed to gradually decrease over time, see fig. 8, and slightly recover after the UCN-production volume was refilled with isopure helium. Part of this change was correlated to a gradual increase in vapor pressure and temperature of the isopure helium, see fig. 9, presumably caused by the gradually dropping helium level in the production volume.

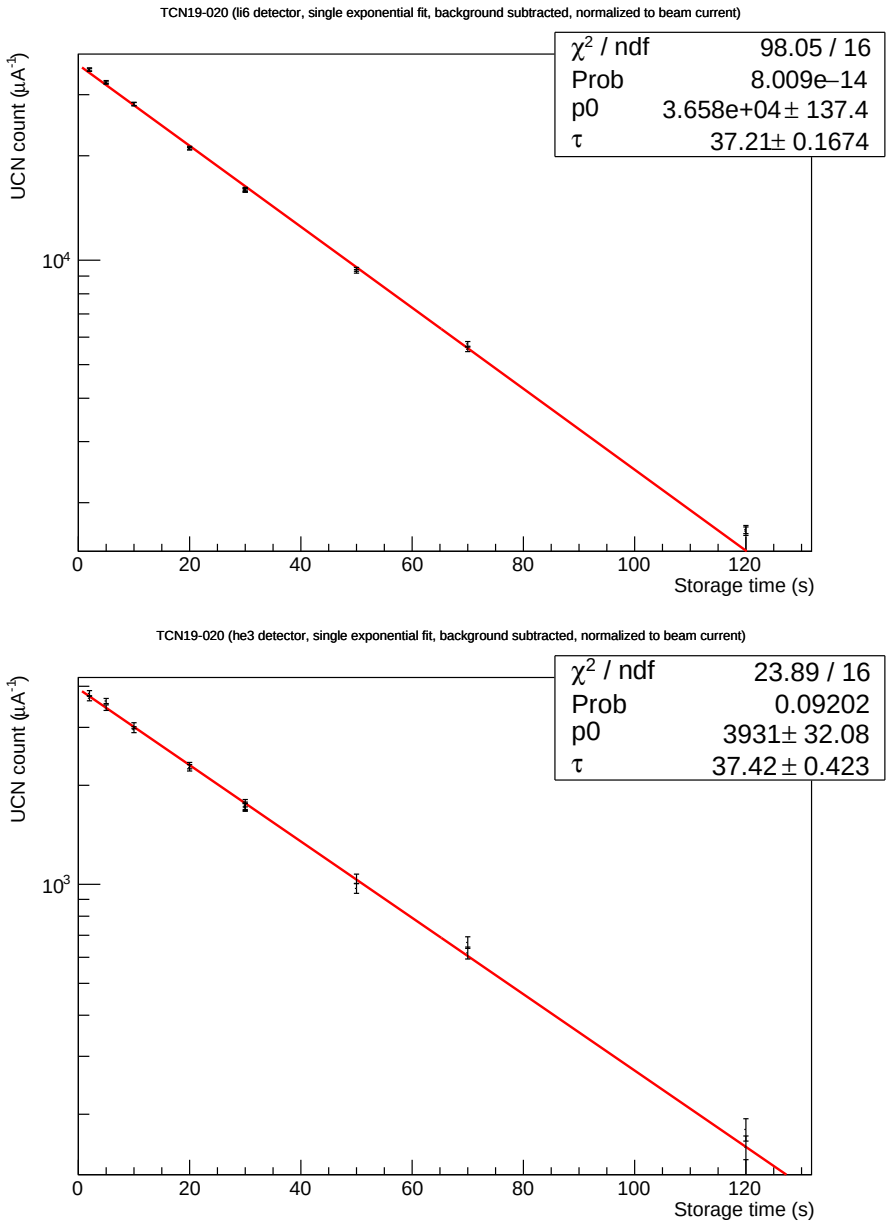

Figure 7: Number of UCN detected in the Li6 detector (top) and the He3 detector (bottom) divided by average beam current, after different storage times during one of the regular storage-lifetime experiments (TCN18-015, run 1019). A single exponential fit determines the storage lifetime.

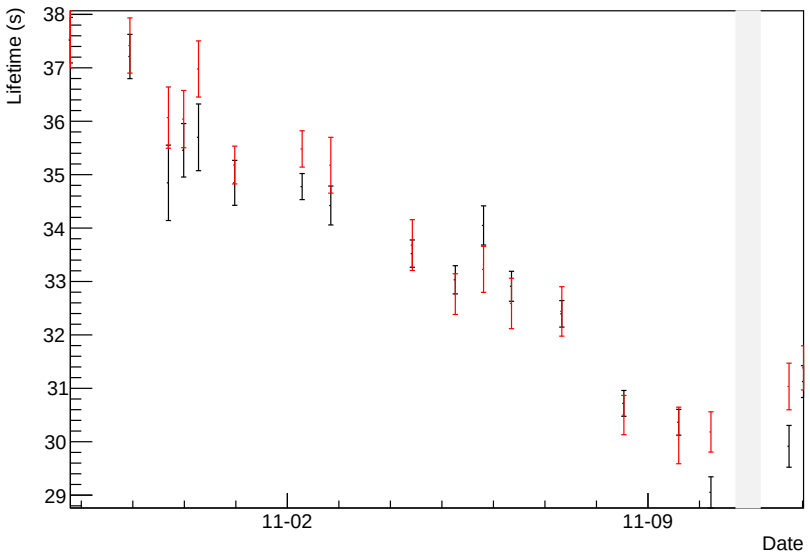

Figure 8: Storage lifetimes on different dates determined from an exponential fit to the UCN counts in the Li6 detector (black) and the He3 detector (red) during the regular storage-lifetime measurements. The grey areas indicate when the production volume was refilled with isopure helium.

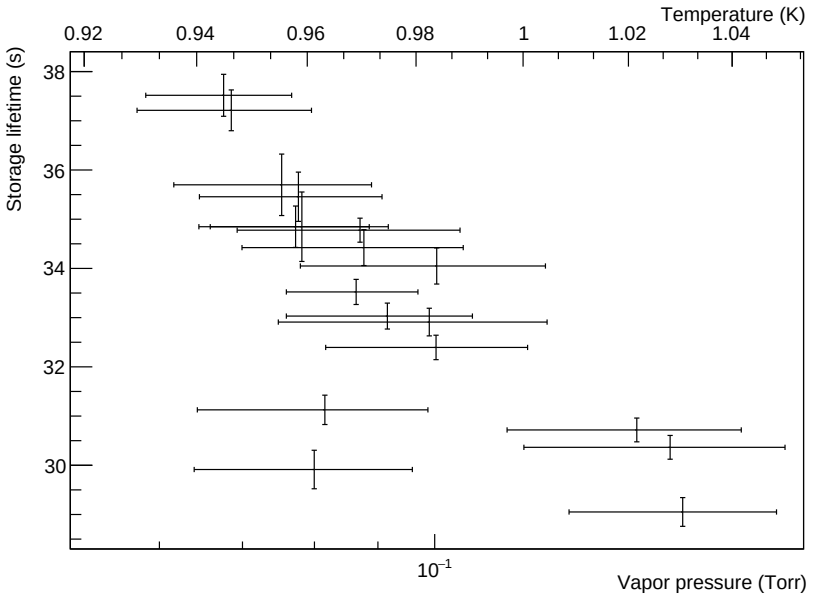

Figure 9: Correlation of storage lifetimes with vapor pressure, measured with the Li6 detector. The two measurements at the bottom left were performed after the isopure-helium refill.

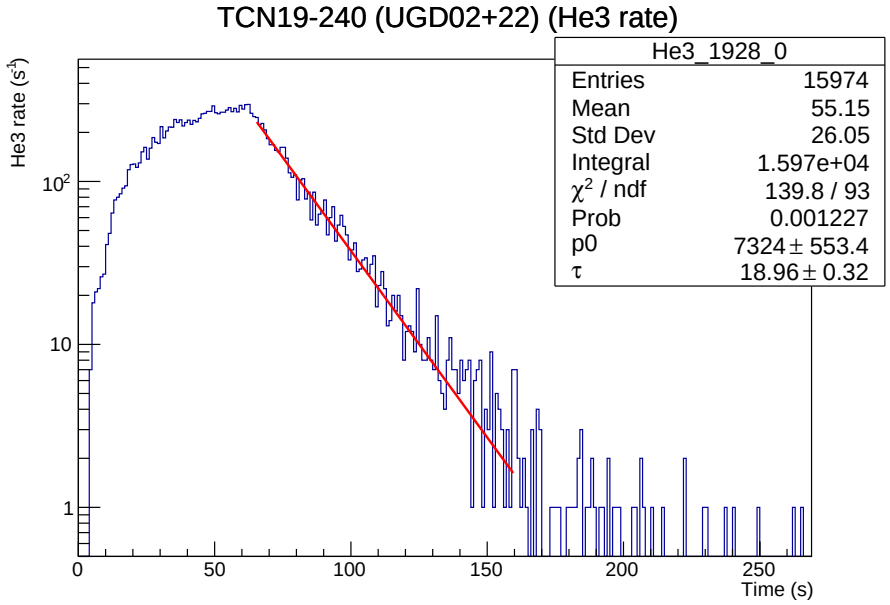

Figure 10: Rate in the He3 detector during a measurement of storage lifetime in a guide component. The rate detected after the irradiation is a measure of the UCN density filled into the guide component. An exponential fit determines the storage lifetime between IV1 and IV2.

5 Storage lifetime in guide components

To determine the storage lifetime in different guide components we ran experiments with three periods per cycle. An irradiation period, where UCN are produced and filled into the component, with the valve IV3 to the detector closed. A storage period, where the irradiation is stopped and all the UCN valves are closed. And a counting period, where the valve to the detector is opened to count the UCN remaining in the component. The He3 detector again serves as monitor detector, measuring the UCN density and storage lifetime in the volume between IV1 and IV2.

UCN remaining in the component after storage are counted with the Li6 detector. The average background determined during the storage period is subtracted using equations (5)–(6) and then normalized using the counts in the He3 detector after the irradiation ended, see fig. 10. The He3 counts are accumulated over the minimal duration of a measurement cycle with 0 s storage time, i.e. the counting time (typically 120 s).

This is repeated for several different storage times. The background-corrected, normalized number of detected UCN is assumed to drop exponentially with storage time. The storage lifetime τ_s is determined with a single exponential fit, see fig. 11. We excluded cycles with a storage time of 0 s (i.e. valve to the detector

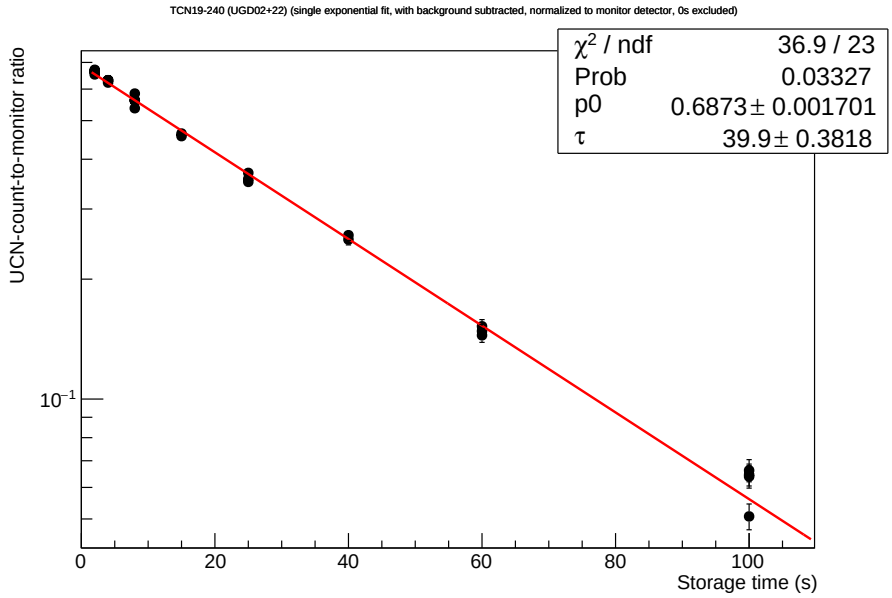

Figure 11: Background-corrected and normalized number of UCN detected in the Li6 detector after different storage times in guides UGD22 and UGD2 between valves IV2 and IV3 (TCN18-081). Cycles with a storage time of 0 s are excluded from the single exponential fit.

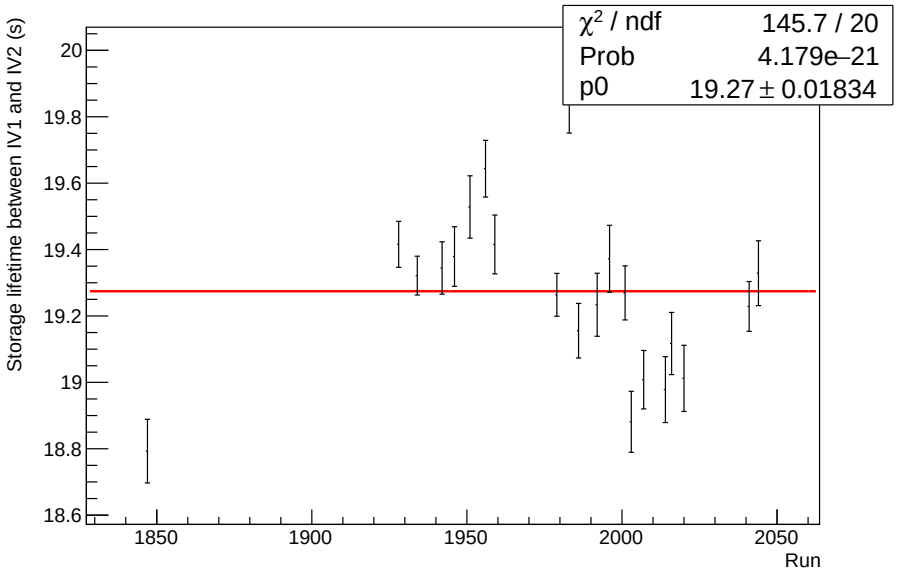

Figure 12: Storage lifetime between IV1 and IV2, measured with the pinhole method. The red line shows the average over all runs where this guide section was unchanged. The first three runs where performed with IV2 flipped, giving higher storage lifetimes. The last two runs were performed in the higher position, resulting in a softer UCN spectrum and longer storage lifetimes.

opening at the same time as the valve(s) to the source closing) from the fit, since UCN could simply be transmitted through both still partially open valves and not have been stored at all.

An exponential fit to the rate in the He3 rate can also confirm the measurements of storage lifetime between IV1 and IV2 that are used to normalize the transmission measurements. These lifetimes are slightly longer than in the transmission experiments, between 18.8 s and 19.8 s, probably due to the longer measurement time, but the overall variation of 1 s is similar, see fig. 12.

5.1 Excluded cycles

Individual cycles are excluded from the analyzed transmission data if

- no beam data was available (4 cycles);
- the beam current dropped below 0.8 µA (20 cycles);
- the beam current fluctuated by more than 0.02 µA (1 cycle);
- the last period does not contain any Li6 events, i.e. the run was aborted at some point during this cycle (17 cycles);

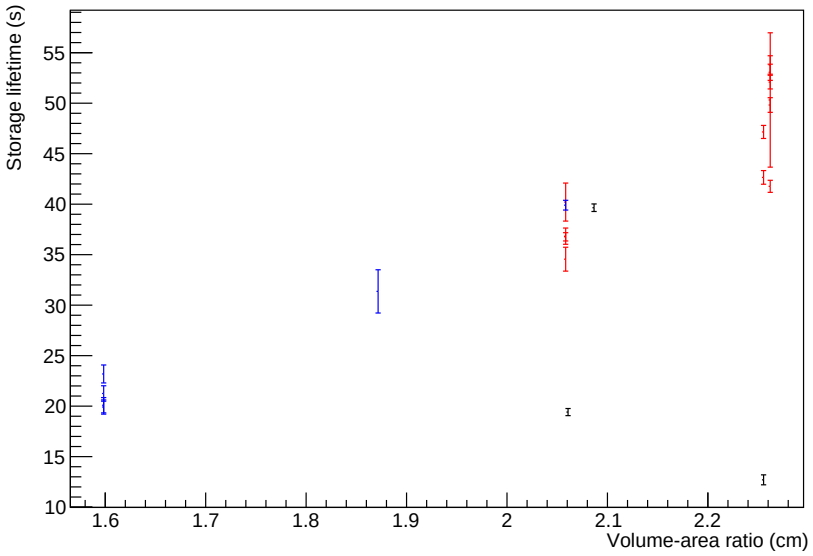

Figure 13: Correlation of storage lifetime in guide components with their volume-to-surface ratio. *Blue*: bare stainless steel components. *Red*: NiP-plated components. *Black*: Copper, black NiP, and combination of steel and NiP.

- IV1 never opened (0 cycles);
- the He3 detector detected less than 1000 UCN during irradiation (0 cycles);
- the Li6 detector detected a large background rate above 10 Hz during the irradiation or background period (3 cycles).

In total, 45 out of 456 cycles had to be excluded.

5.2 Results

The results, see table 4, seem much more stable than in 2018, with almost all fitting nicely to an exponential with a reduced $\chi^2 < 2$. The cases with larger χ^2 can be traced back to large variations in detector background or, in the case of TCN19-010B, to instabilities in the source.

Except for the copper and black-NiP-coated guides, the storage lifetimes are linearly correlated with their volume-to-surface ratio, see Fig. 13. Storage lifetime is not correlated with roughness, see Fig. 14—the rougher guide UGD36 had only a slightly shorter storage lifetime as the other guides coated by ChemProcessing (UGD37/39).

Table 4: Results of storage experiments in different guide components. All measurements were performed with the listed guides between IV2 and IV3 with their O-rings pointing towards each other and a 90° elbow downstream of IV3. The χ^2 gives an indication of how well the data fits the single exponential. The struck-out entries were affected by large variations of the Li6 background or, in the last row, by instability of the source.

Experiment	Runs	τ_s	χ^2/ν	Description
TCN19-010	1847, 1850	~~34.6 ± 0.6~~	4.20	UGD19+22
TCN19-240	1928	39.9 ± 0.4	1.60	UGD02+22
TCN19-250	1934, 1938	39.7 ± 0.3	1.65	UGD02+19+22
TCN19-260	1942	~~31.4 ± 0.8~~	6.57	UGD22
TCN19-280v1	1946	20.1 ± 0.8	0.69	vent spider
TCN19-280v2	1951	21.3 ± 0.8	0.67	vent spider with plunger full in
TCN19-280v3	1956	19.9 ± 0.7	1.06	vent spider with pluger cycled
TCN19-280v4	1959	23.2 ± 0.8	1.14	vent spider with plunger full in
TCN19-010D	1979, 1980	36.8 ± 0.4	1.13	UGD19+22
TCN19-270	1983	19.4 ± 0.4	0.91	UGD13+14+15+22
TCN19-120	1986	53.8 ± 0.6	2.08	UGD37+22 (95mm Al-NiP)
TCN19-121	1992	49.8 ± 0.6	1.40	UGD36+22 (95mm Al-NiP rough)
TCN19-123	1996	53.1 ± 0.6	1.57	UGD39+22 (95mm Al-NiP)
TCN19-100	2001	47.2 ± 0.6	1.30	UGD31+33+22 (95mm SS-NiP)
TCN19-101	2003	12.7 ± 0.3	2.78	UGD30+32+22 (95mm SS-black NiP)
TCN19-120A	2007	52.09 ± 0.7	0.98	UGD37+22 (95mm Al-NiP)
TCN19-102	2014	42.7 ± 0.5	1.56	UGD34+35+22 (95mm Al-NiP)
TCN19-124	2016	41.8 ± 0.6	1.09	UGD40+22 (95mm SS-NiP smooth)
TCN19-010E	2020	36.8 ± 0.6	2.02	UGD19+22
TCN19-120B	2041, 2043	~~50.3 ± 0.5~~	147	UGD37+22
TCN19-010B	2044, 2045	~~34.6 ± 0.6~~	4.2	UGD19+22

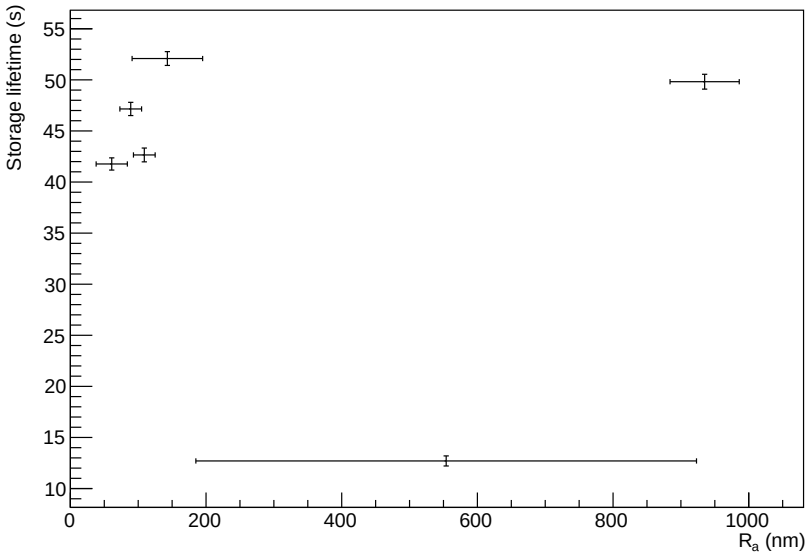

Figure 14: Correlation of storage lifetime in guide components with their roughness R_a.

6 Background rates

We used the storage periods in the storage-lifetime measurements to estimate background rates of the Li6 and He3 detectors. When measuring storage lifetime in the source, both detectors are separated from the source by vacuum-tight valves, so we assumed that no UCN can leak from the source into the detectors. The background rate in the He3 detector proved to be very stable around an average of $(0.0345 \pm 0.0022)\,\mathrm{s}^{-1}$, see fig. 15. The Li6 detector had a much higher background rate of $(1.543 \pm 0.012)\,\mathrm{s}^{-1}$, slightly lower than in 2018, but still 45 times more than the He3 detector, and showed more fluctuations between measurements. It seemed to be correlated with the beam current in 1A. The first measurement of storage in a guide in fig. 16 was performed at a 1A beam current of 38 µA.

During storage-lifetime measurements in guide components and transmission measurements, the He3 detector is always connected to the source, but the storage periods can be used to determine background in the Li6 detector, see table 5.

While the target was irradiated with protons, both detectors saw a significant increase in background rate. To estimate the increase, we subtracted the previously determined background from the UCN counted during the irradiation period, and normalized the result to beam current. The He3 detector saw an increase in background rate of 190 % at 1 µA, the Li6 detector an increase of

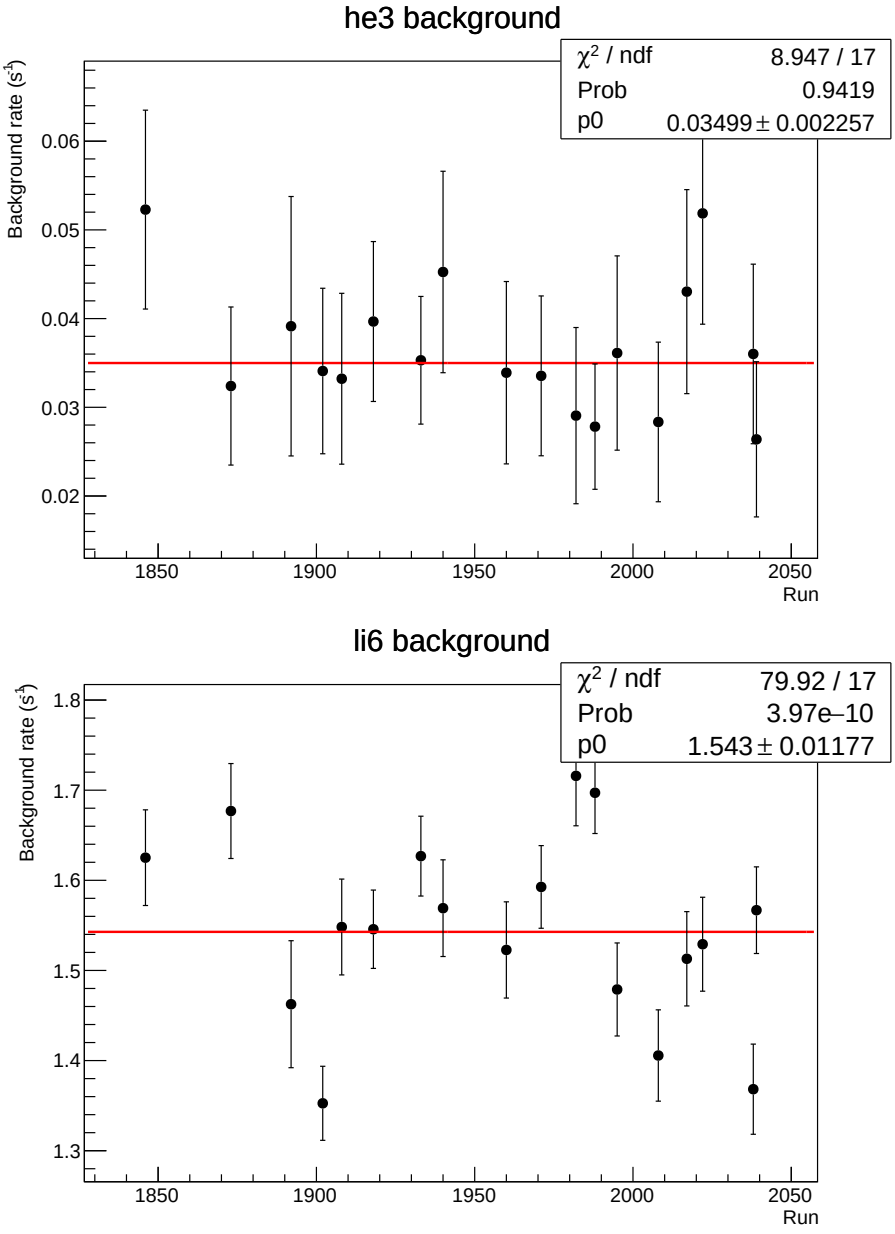

Figure 15: Background rates in the He3 (top) and Li6 (bottom) detectors averaged over all storage periods of each measurement of storage lifetime in the source. The red line indicates the overall average. The first three runs, where the Li6 detector was connected to the DAQ but not used for the actual measurement, were excluded from the overall average.

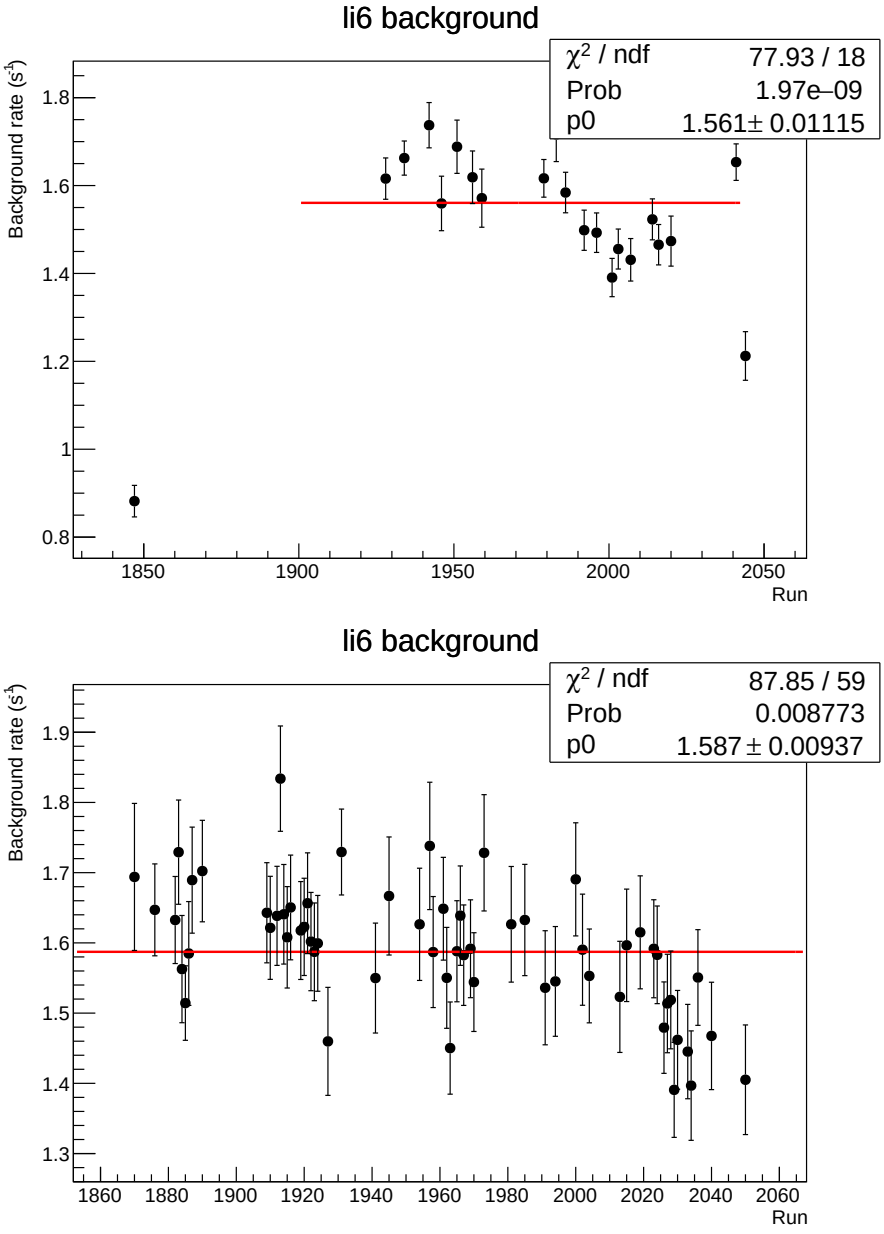

Figure 16: Background rate in the Li6 detector averaged over all storage periods during measurements of storage lifetime (top) or transmission (bottom) of a guide component. The first and last data point in the top graph were taken while beamline 1A operated at lower beam current and are excluded from the average.

Table 5: Background rates averaged over all cycles of each measurement type.

Experiment	Detector	Background (s^{-1})	Additional during irrad. ($s^{-1}\,\mu A^{-1}$)
Storage lifetime	He3	0.0345 ± 0.0022	0.0653 ± 0.0023
Storage lifetime	Li6	1.543 ± 0.012	4.264 ± 0.018
Storage lifetime guides	Li6	1.561 ± 0.011	4.158 ± 0.016
Transm. w/ pre-storage	Li6	1.587 ± 0.009	4.308 ± 0.007
Transmission	Li6	–	4.267 ± 0.019

280 %, see table 5.